Thermobaricity in the Transition Zones between Alpha and Beta Oceans

KIAL D. STEWART

Research School of Earth Sciences, Australian National University, and Australian Research Council Centre of Excellence for Climate System Science, Canberra, Australian Capital Territory, Australia

THOMAS W. N. HAINE

Department of Earth and Planetary Sciences, The Johns Hopkins University, Baltimore, Maryland

(Manuscript received 11 January 2016, in final form 14 March 2016)

ABSTRACT

The role of the ocean in Earth's climate is fundamentally influenced by the locally dominant stratifying property (heat or salt), which in turn can be used to categorize the ocean into three classes: alpha, beta, and transition zone oceans. Alpha and beta oceans are regions where the stratification is permanently set by heat and salt, respectively. Transition zone oceans exist between alpha and beta oceans and are regions where the stratification is seasonally or intermittently set by heat or salt. Despite their large ranges of temperature and salinity, transition zone oceans are the most weakly stratified regions of the upper oceans, making them ideal locations for thermobaric effects arising from the nonlinear equation of state of seawater. Here a novel definition and quantification of alpha, beta, and transition zone oceans is presented and used to analyze 4 years (2010–13) of hydrographic data developed from the Argo profiling float array. Two types of thermobaric instabilities are defined and identified in the hydrographic data. The first type arises from the vertical relocation of individual water parcels. The second type is novel and relates to the effect of pressure on the stratification through the pressure dependence of the thermal expansion coefficient; water that is stably stratified for one pressure is not necessarily stable for other pressures. The upper 1500 m of the global ocean is composed of 67% alpha, 15% beta, and 17% transition zone oceans, with 5.7% identified as thermobarically unstable. Over 63% of these thermobarically unstable waters exist in transition zone oceans, suggesting that these are important locations for efficient vertical transport of water-mass properties.

1. Introduction

The locally dominant stratifying property is an important, yet often overlooked, dynamical attribute of the global oceans. Whether a region is permanently stratified by temperature (referred to as an alpha ocean; predominantly low latitudes) or salinity (a beta ocean; predominantly high latitudes) fundamentally alters the role it plays in Earth's climate and biogeochemical systems (see Carmack 2007, and references therein). For instance, open ocean sea ice formation can only occur over a beta ocean where a permanent halocline prevents deep thermal convection. Sea–air fluxes of heat, freshwater, momentum, potential vorticity, CO_2, and other tracers are all affected by the upper-ocean stratification and the respective contributions from temperature and salinity (e.g., Fedorov et al. 2004; Polyakov et al. 2013; Franco et al. 2014). The nature of the stratification, especially within the euphotic zone, is of foremost importance to the local ecology (McLaughlin and Carmack 2010). Distinguishing between regions stratified by heat and regions stratified by salt is a crucial oceanographic endeavor (as noted by Rooth 1982).

Separating the alpha and beta oceans are boundary regions known as transition zones (following Sverdrup et al. 1942). These transition zones span hundreds of kilometers in meridional extent, predominantly in subpolar latitudes. They alternate between being stratified by heat and salt on a seasonal or intermittent basis. Although these transition zone oceans contain large horizontal gradients of temperature and salinity, the heat and salt contributions to the stratification are largely density compensating, resulting in these regions

Corresponding author address: Kial D. Stewart, Research School of Earth Sciences, Australian National University, 142 Mills Rd., Canberra ACT 2600, Australia.
E-mail: kial.stewart@anu.edu.au

DOI: 10.1175/JPO-D-16-0017.1

exhibiting the weakest stratification of all the oceans, and, importantly, a regional surface density maximum (e.g., Roden 1970). Their weak stratification makes transition zone oceans ideal locations for efficient vertical exchange of water-mass properties across the ocean thermocline.

Among the various mechanisms for coupling waters across the thermocline are two that arise from nonlinearities in the equation of state of seawater (Fig. 1a), namely, cabbeling and thermobaricity (Fofonoff 1961; McDougall 1987). Cabbeling refers to the densification of water masses through the mixing of waters with different temperatures and salinities. This effect is reflected in the curvature of isopycnals in temperature–salinity space (Figs. 1a,b); in this coordinate frame the mixed product water exists on the straight line connecting the source waters, ensuring the density of the product is always greater than the average density of the sources. Thermobaricity arises from the pressure dependence of the thermal expansion coefficient: two water masses of equal density but different temperature and salinity will not remain of equal density following a change of pressure. In other words, they are not equally compressible and have different sound speeds: cold, freshwater is more compressible (lower sound speed) than warm, salty water. This effect is apparent through the pressure dependence of the isopycnal curvature in temperature–salinity space (Figs. 1a,c).

The cabbeling and thermobaricity mechanisms are important water-mass transformation processes responsible for as much as 20% of the downward diapycnal transport of the global oceans (e.g., Klocker and McDougall 2010) and crucial for the formation of mode and intermediate waters (see, e.g., You et al. 2000; Talley and Yun 2001; Nycander et al. 2015). Additionally, they have been identified as contributors of available potential energy for maintaining the meridional overturning circulation of the global oceans (Urakawa et al. 2013) through the processes depicted schematically in Figs. 1b and 1c. Their importance for modifying the density field is able to be quantified using the international Thermodynamic Equation of Seawater 2010 (TEOS-10) and associated software packages (IOC et al. 2010). The cabbeling contribution is related to the square of the conservative temperature (Θ) difference between the mixed water masses, which is sign definite to only densify waters. The thermobaric contribution is related to the scalar product of the conservative temperature and pressure (p) perturbations, which is not sign definite and both lightens and densifies waters.

In the transition zones, planes of constant locally referenced potential density tend to strongly tilt, resulting in large along-plane gradients of pressure, which, combined with the wide distribution of temperatures, imply these waters are prime locations for thermobaric processes. An abundance of thermobaricity would increase the efficiency of vertical exchange in the transition zone oceans and motivates this investigation into whether, and by how much, the transition zone oceans are more thermobarically active than the rest of the oceans.

Detecting these nonlinear effects in global ocean observations is challenging. Cabbeling is a dynamic process involving the mixing of water masses. Identifying this effect requires detailed knowledge of mixing events (source water masses, spatial extent, turbulence, duration, etc.), which might be obtainable for high-resolution circulation models, but are rarely available in global ocean observations. While it might be possible to estimate such details of mixing events from bulk measurements, the resulting estimates of cabbeling in global ocean observations would be overly dependent on these mixing estimates. In contrast, thermobaricity is a conditional instability that can be identified by examining the sensitivity of stratification to pressure changes. However, thermobaric processes have small vertical scales and involve dynamical instability; hence, they are relatively short lived. Additionally, many common global ocean hydrographic climatologies and reanalyses impose gravitational (static) stability for their gridded products, thus obscuring much of their thermobaricity. Previous studies identifying thermobaric instabilities have employed high-resolution observations from specific regions (e.g., McPhee 2000, 2003; Carmack et al. 2012). The Argo array of profiling floats offers near-global upper-ocean temperature and salinity data at unprecedented vertical resolution, making their data ideal for diagnosing thermobaric processes and quantifying their distribution and importance.

Here, 4 years (2010–13) of hydrographic data developed primarily from the Argo profiling float array are analyzed to partition the upper global ocean into its alpha, beta, and transition zone components and to quantify thermobaric instabilities. This analysis reveals the distributions of ocean classes to be complex in horizontal and vertical structure. Thermobaric instabilities overwhelmingly occur in transition zone oceans. This finding, together with their weak stratification, suggests that the transition zones operate as conduits for the efficient vertical exchange of water-mass properties.

2. Methodology

a. Alpha, beta, and transition zone oceans

The squared buoyancy frequency N^2 (s^{-2}) measures density stratification and is defined by the TEOS-10 as

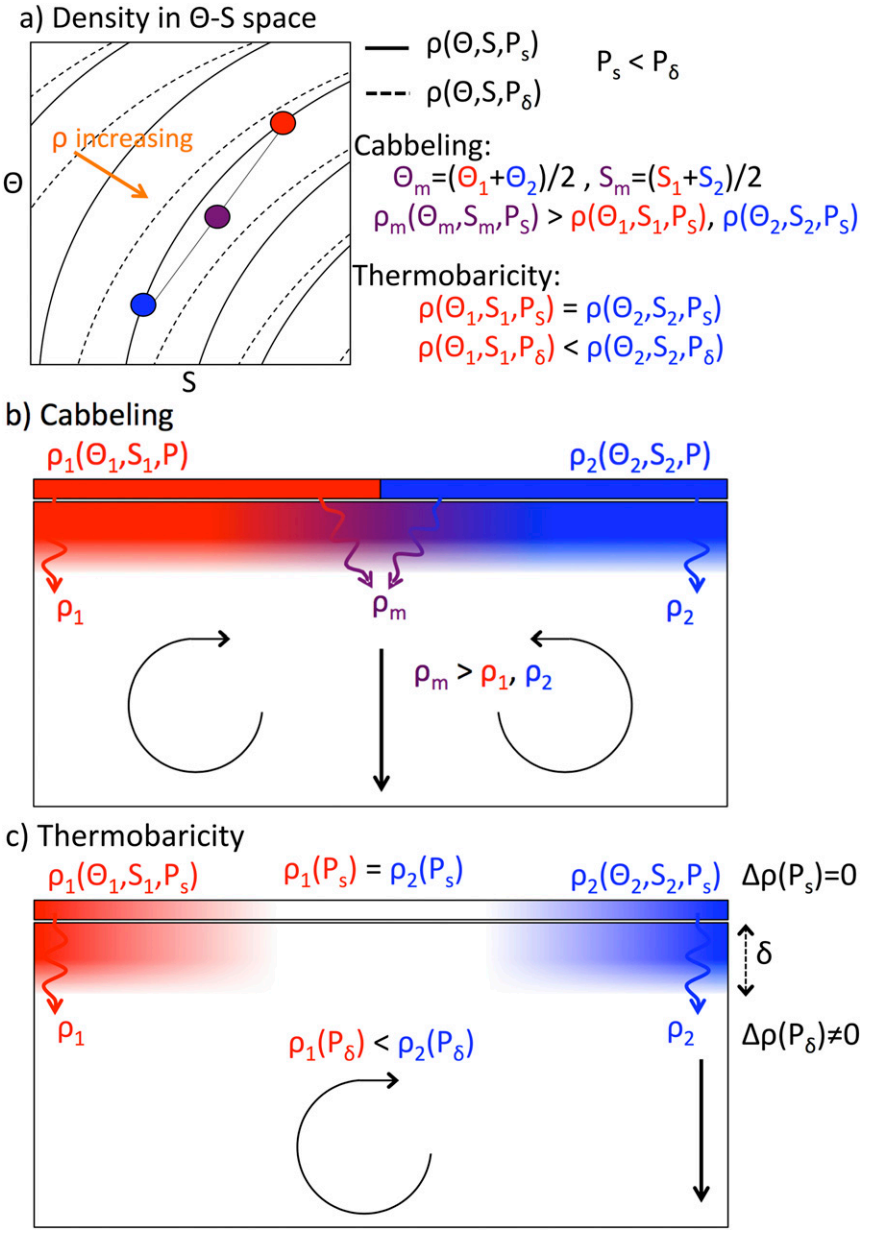

FIG. 1. A schematic of the two dominant physical consequences of the nonlinearity of the equation of state of seawater. (a) Consider the two parcels shown in blue and red with equal density ρ but of different temperature Θ and salinity S. If mixed in equal portions, their product, represented in magenta, is of average temperature and salinity but, because of isopycnal curvature in Θ–S space, is at greater than the average density of the two parcels; this process is referred to as cabbeling. In addition, the isopycnal curvature is a function of pressure, so the two isopycnic parcels at one (low) pressure P_s are no longer isopycnic at a different (greater) pressure P_δ; this process is referred to as thermobaricity. (b) Cabbeling: consider a control volume whose surface is relaxed to an isopycnal with large horizontal gradients of Θ and S; horizontal diffusion produces water of intermediate (Θ, S) but greater density, thus generating available potential energy and sinking, as shown. (c) Thermobaricity: if the surface isopycnal has weak horizontal gradients of Θ and S, vertical diffusion will bring the surface (Θ, S) properties to pressures where they are no longer isopycnic, leading to a horizontal density gradient at this pressure and thus available potential energy and overturning, as shown.

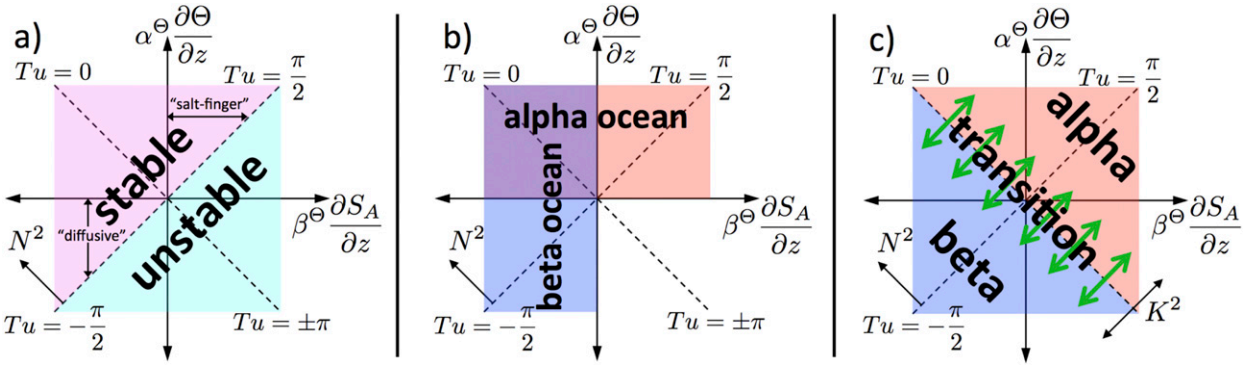

FIG. 2. (a) The classical diagram for the Turner angle depicting the regions of gravitational stability ($|\mathrm{Tu}| < \pi/2$) and instability ($|\mathrm{Tu}| > \pi/2$), the diffusive ($-\pi/2 < \mathrm{Tu} < -\pi/4$) and salt-finger ($\pi/4 < \mathrm{Tu} < \pi/2$) double-diffusive convection regimes, and the buoyancy frequency N^2 [(1)] increasing to the upper left. (b) The nominal definition of alpha and beta oceans described by Carmack (2007); by this definition, the doubly stable region of $|\mathrm{Tu}| < \pi/4$ is classified as both alpha and beta oceans simultaneously and there is no classification for the unstable regime $|\mathrm{Tu}| > 3\pi/4$. (c) The spice stratification or spice frequency K^2 [(5)], which increases to the upper right, offers an exact, mutually exclusive definition of alpha ($\overline{K^2} - \sigma_{K^2} > 0$), beta ($\overline{K^2} + \sigma_{K^2} < 0$), and transition zone ($|\overline{K^2}| - \sigma_{K^2} < 0$) oceans.

$$N^2 = g\left(\alpha^\Theta \frac{\partial \Theta}{\partial z} - \beta^\Theta \frac{\partial S_\mathrm{A}}{\partial z}\right), \tag{1}$$

where g is the acceleration due to gravity ($\mathrm{m\,s^{-2}}$), Θ is the conservative temperature (°C), S_A is the absolute salinity ($\mathrm{g\,kg^{-1}}$), and z is the depth (m, negative downward). The thermal expansion coefficient α^Θ ($^\circ\mathrm{C}^{-1}$) and the saline contraction coefficient β^Θ ($\mathrm{g^{-1}\,kg}$) are given by

$$\alpha^\Theta = -\frac{1}{\rho}\frac{\partial \rho}{\partial \Theta}\bigg|_{S_\mathrm{A},p} \quad \text{and} \quad \beta^\Theta = \frac{1}{\rho}\frac{\partial \rho}{\partial S_\mathrm{A}}\bigg|_{\Theta,p}, \tag{2}$$

respectively, where ρ is the in situ density ($\mathrm{kg\,m^{-3}}$) and p is the sea pressure (Pa), which is defined as the absolute pressure P less one standard atmosphere, $P_0 \equiv 101\,325$ Pa ($p \equiv P - P_0$). Both α^Θ and β^Θ are positive for the range of parameters relevant to the global ocean.[1] The superscript Θ, as used by the TEOS-10, indicates terms that have been calculated using Θ and S_A. This formulation of the buoyancy frequency is convenient for comparing the respective contributions of temperature and salinity to the total stratification.

The TEOS-10 also evaluates the Turner angle Tu (rad, see Ruddick 1983) as

$$\mathrm{Tu} = \tan^{-1}\left(\alpha^\Theta \frac{\partial \Theta}{\partial z} + \beta^\Theta \frac{\partial S_\mathrm{A}}{\partial z}, \alpha^\Theta \frac{\partial \Theta}{\partial z} - \beta^\Theta \frac{\partial S_\mathrm{A}}{\partial z}\right), \tag{3}$$

which is traditionally used as an indicator of double-diffusive potential [e.g., see climatological atlas of Tu in You (2002)], and more recently to attribute density variations to temperature or salinity changes (Johnson et al. 2012). The Turner angle ranges over $-\pi < \mathrm{Tu} < \pi$ and is convenient to view in $(\alpha^\Theta \partial\Theta/\partial z,\ \beta^\Theta \partial S_\mathrm{A}/\partial z)$ space (hereinafter referred to as "Turner space"; Fig. 2a). Here, the water column is statically stable to infinitesimal perturbations for $-\pi/2 < \mathrm{Tu} < \pi/2$ (i.e., $N^2 > 0$) and doubly stable for $-\pi/4 < \mathrm{Tu} < \pi/4$ (i.e., $\alpha^\Theta \partial\Theta/\partial z > 0$ and $\beta^\Theta \partial S_\mathrm{A}/\partial z < 0$).[2] For $\mathrm{Tu} > 0$, the contribution of temperature to the stratification is dominant; for $\mathrm{Tu} < 0$, the contribution of salinity is dominant. The Turner angle is particularly useful for studies of double-diffusive convection as the "salt finger" and "diffusive" regimes occur for $\pi/4 < \mathrm{Tu} < \pi/2$ and $-\pi/2 < \mathrm{Tu} < -\pi/4$, respectively, reflecting regimes where the stratification is overall stable but is composed of an unstable salinity or temperature contribution. It will be shown that these salt-finger and diffusive regimes exist near the gravitationally unstable boundaries of alpha and beta oceans, respectively, and that these double-diffusive processes operate to bring the water column toward the doubly stable region of $-\pi/4 < \mathrm{Tu} < \pi/4$.

Carmack (2007) defines alpha and beta oceans as permanently stably stratified by temperature and salinity, respectively. Using the TEOS-10, these definitions for alpha and beta oceans can be expressed as

$$\alpha^\Theta \frac{\partial \Theta}{\partial z} > 0 \quad \text{and} \quad \beta^\Theta \frac{\partial S_\mathrm{A}}{\partial z} < 0, \tag{4}$$

[1] For those small regions where α^Θ is negative ($S_\mathrm{A} \lesssim 24\,\mathrm{g\,kg^{-1}}$), the framework below still applies.

[2] Throughout, instabilities arising from horizontal gradients in density or momentum are neglected (see, e.g., Haine and Marshall 1998).

respectively. In terms of Turner angle, these definitions are $-\pi/4 < \mathrm{Tu} < 3\pi/4$ and $-3\pi/4 < \mathrm{Tu} < \pi/4$, respectively (Fig. 2b). These definitions are not mutually exclusive, however, as they are only based on the signs of the contributions to the stratification by temperature and salinity. Therefore, it is possible for a region to be classified as simultaneously an alpha and a beta ocean (viz., $|\mathrm{Tu}| < \pi/4$). Even though this doubly stable region is likely to be thermodynamically quiescent, knowledge of whether the stratification is predominantly set by heat or salt is crucial for predicting response to changing conditions, for instance. Additionally, these definitions do not cover the doubly unstable case where neither condition in (4) applies (viz., $|\mathrm{Tu}| > 3\pi/4$).

Here, the definitions for alpha and beta oceans are refined to account for the relative sizes of the contributions to the stratification by temperature and salinity. In other words, the proposed definitions are that the vertical density stratifications of an alpha (beta) ocean are dominated by heat (salt). The Turner angle contains this information (Fig. 2c): regions where the Turner angle is permanently positive are alpha oceans and where it is permanently negative are beta oceans. Specifically, these simple definitions could be expressed for alpha (beta) oceans as permanently $0 < (-)\mathrm{Tu} < \pi$. However, while these strict Tu-based definitions ensure mutual exclusivity between alpha and beta oceans, they fail to account for weakly stratified regions where Tu changes sign seasonally or intermittently. Therefore, further refinement is needed to account for the variability of ocean stratifications.

This refinement is achieved by employing the vertical gradient of "spice," K^2 (s^{-2}), where

$$K^2 = g\left(\alpha^\Theta \frac{\partial \Theta}{\partial z} + \beta^\Theta \frac{\partial S_\mathrm{A}}{\partial z}\right). \tag{5}$$

The K^2 variable is referred to as the "spice stratification" or the "spice frequency," in keeping with the name for N^2 (Munk 1981), although it is important to note that K^2 is sign indefinite and K does not quantify the frequency of a physical oscillation. Contours of K^2 are normal to contours of N^2 in Turner space (Fig. 2), so they provide a complementary coordinate basis to describe the vertical stratification (Fig. 2c). In particular,

$$\mathrm{Tu} = \tan^{-1}(K^2, N^2), \tag{6}$$

$$\alpha^\Theta \frac{\partial \Theta}{\partial z} = \frac{1}{2g}(K^2 + N^2), \quad \text{and} \tag{7}$$

$$\beta^\Theta \frac{\partial S_\mathrm{A}}{\partial z} = \frac{1}{2g}(K^2 - N^2). \tag{8}$$

For a time series of hydrographic data, the degree of alpha- or beta-ness of a region is quantified by the time-mean spice stratification $\overline{K^2}$ (overbar indicates time mean): alpha (beta) oceans will have positive (negative) $\overline{K^2}$. Furthermore, the variability of the ocean type is quantified by the variability of K^2, characterized here as the standard deviation of the spice stratification σ_{K^2} (positive definite), given by

$$\sigma_{K^2} = \sqrt{\overline{(K^2)^2} - \overline{K^2}\,\overline{K^2}}. \tag{9}$$

These two terms $\overline{K^2}$ and σ_{K^2} provide exact and mutually exclusive definitions for three ocean types:

$$\text{alpha ocean: } \overline{K^2} - \sigma_{K^2} > 0, \tag{10}$$

$$\text{beta ocean: } \overline{K^2} + \sigma_{K^2} < 0, \quad \text{and} \tag{11}$$

$$\text{transition zone ocean: } |\overline{K^2}| - \sigma_{K^2} \le 0. \tag{12}$$

These definitions classify the ocean stratifications in a robust statistical way. Definitions of greater complexity can be formulated using other K^2 distribution statistics; such definitions would be tailored to suit the dataset and application. For instance, employing a reduced averaging period to calculate $\overline{K^2}$ and σ_{K^2} enables investigations into secular changes between the ocean types. Nevertheless, this basic definition [(10)–(12)] suits the needs of the present study.

Finally, for completeness, note that the stability ratio R_ρ (IOC et al. 2010) is the ratio of the heat-to-salt contributions to the stratification,

$$R_\rho = \frac{\alpha^\Theta \dfrac{\partial \Theta}{\partial z}}{\beta^\Theta \dfrac{\partial S_\mathrm{A}}{\partial z}} = \frac{K^2 + N^2}{K^2 - N^2} = -\tan\left(\mathrm{Tu} + \frac{\pi}{4}\right). \tag{13}$$

The stability ratio R_ρ does not distinguish alpha from beta oceans; for example, both the alpha ocean ($\mathrm{Tu} = \pi/2$) and the beta ocean ($\mathrm{Tu} = -\pi/2$) have the same $R_\rho = 1$.

b. *Identifying thermobaric instabilities*

Here, two types of thermobaric instabilities are presented. The first (type I) involves the vertical relocation of a water parcel through a gravitationally stable stratification from one pressure to another, with the associated change in density resulting in the relocated water becoming gravitationally unstable and thus triggering a convective thermobaric instability (Fig. 3a). Such a vertical relocation could arise from wind-driven mixed layer overturnings or entrainment into sinking plumes. The second (type II) focuses on the effect of pressure on the stratification itself (Fig. 3b). Considering the strong pressure dependence of thermal expansion coefficient α^Θ, and its important relation with the thermal

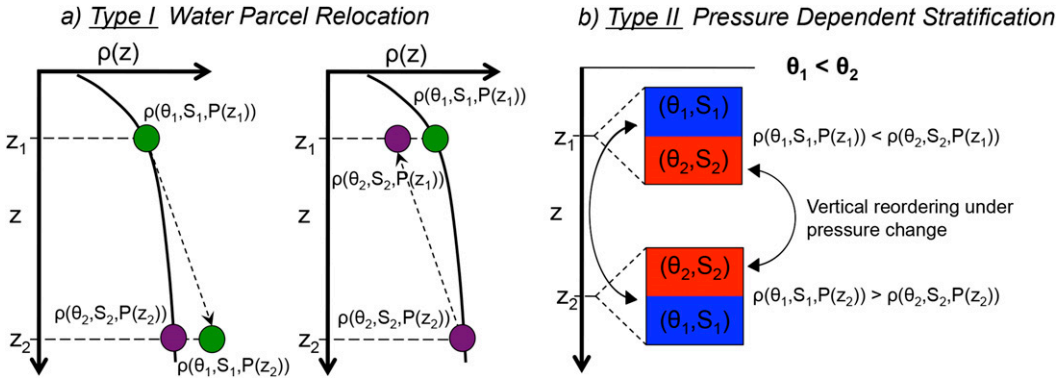

FIG. 3. A schematic for the two types of thermobaric instabilities examined here. (a) Type I water parcel relocation: consider the vertical relocation of a water parcel through a statically stable stratification to a region of higher pressure (left, green). The increased pressure will increase the density of the parcel, and if this increased density is greater than that of the surrounds (magenta) will lead to thermobaric (downward) convection. Alternatively, if a parcel is relocated to a region of reduced pressure (right, magenta), and the decreased density is less than the surrounds (green), it will lead to thermobaric (upward) convection. (b) Type II pressure-dependent stratification: consider a statically stable beta ocean (top) that undergoes an increase in pressure. The overlying cooler water is more compressible than the underlying warmer water and thus will be densified more; for a sufficiently large pressure increase the overlying water can become denser than that underlying, leading to the vertical reordering of the stratification. For an alpha ocean (bottom), it is a decrease in pressure that can lighten the underlying cooler water more than the overlying warmer water and lead to the thermobaric instability.

contribution to the density stratification, a gravitationally stable stratification at one pressure is not necessarily stable at another pressure. Type II thermobaric instabilities might be triggered by pressure perturbations through internal or surface waves. Other processes may be capable of generating thermobaric instabilities (e.g., see discussions in Hieronymus and Nycander 2015).

1) WATER PARCEL RELOCATION: TYPE I

Consider a gravitationally neutral or weakly stable ($N^2 \gtrsim 0$) water column with two parcels of equal density, but different temperature and salinity, at depth $z + \Delta z$. Through thermobaricity, any perturbation in pressure Δp (for instance, through a vertical relocation from depth $z + \Delta z$ to z) will result in the parcels no longer being of equal density. Occasionally, the new density of a vertically relocated water parcel is gravitationally unstable with respect to its surrounds, triggering a convective thermobaric instability that is available to drive motion (e.g., see description and schematics in Garwood et al. 1994; Akitomo 1999a,b; McPhee 2003). This thermobaric instability can be triggered in two ways: when the density of water relocated to a *greater* pressure is *denser* than its new surrounds, or when the density of water relocated to a *lesser* pressure is *lighter* than its new surrounds (Fig. 3a). That is, thermobaric instability is possible if

$$\mathrm{sgn}(\Delta p)\Delta\rho(z,\Delta z) > 0, \tag{14}$$

where

$$\Delta\rho(z,\Delta z) = \underbrace{\rho[\Theta(z+\Delta z), S_{\mathrm{A}}(z+\Delta z), p(z)]}_{\text{water relocated from } z+\Delta z \to z} - \underbrace{\rho[\Theta(z), S_{\mathrm{A}}(z), p(z)]}_{\text{ambient water at depth } z}, \tag{15}$$

for $\mathrm{sgn}(x) = x/|x|$ as the sign function. This definition assumes that the vertical displacement over Δz occurs under isentropic and isohaline conditions with no change in the ambient pressure field. The term $\Delta\rho(z, \Delta z)$ is equivalent to Eq. (1) of McPhee (2003) and can be interpreted as the thermobaric tendency of a water parcel: the parcel has stronger thermobaric tendencies if (14) is satisfied with larger $\Delta\rho(z, \Delta z)$ and smaller $|\Delta z|$.[3] This definition for thermobaric instability is referred to here as a type I instability.

It is important to note that thermobaric instabilities are *conditional* instabilities because they require finite amplitude perturbations in pressure, $p(z + \Delta z) - p(z)$, to activate. This is the reason attention is

[3] Conceivably, an analysis akin to those of Hughes et al. (2009), Stewart et al. (2014), or Saenz et al. (2015) could employ vertical profiles of $\Delta\rho(Z, \Delta Z)$ to calculate the potential energy contained within thermobaric instabilities and made available through the triggering of these instabilities. This analysis this is beyond the scope of the present study, however.

restricted to regions that are neutral or weakly stable to infinitesimal vertical perturbations, $N^2 \gtrsim 0$; otherwise, static gravitational instability dominates. Thermobaric instabilities can be identified in hydrographic data by examining the density fields with respect to the criteria of (14). This is achieved via an algorithm that steps through the gravitationally stable regions of the gridded fields and individual float profiles and compares the in situ density [the second term on the right-hand side of (15)] with the in situ local pressure-referenced potential densities of the overlying and underlying water columns [the first term on the right-hand side of (15)]. Specifically, if the potential densities of the overlying (underlying) waters are greater (lesser) than the in situ density, the water parcel is identified as thermobarically unstable. For any given depth of interest z, the water column may contain a range of depths $z + \Delta z$ that contain thermobarically unstable water. More generally, unstable water can be present in multiple disconnected ranges (of both signs) of Δz for each z.

2) PRESSURE-DEPENDENT STRATIFICATION: TYPE II

An alternative, novel diagnostic for identifying thermobaric instabilities considers the effect of pressure on the stratification. This pressure dependence arises primarily from the pressure dependence of the thermal expansion coefficient $\partial\alpha^\Theta/\partial p$, which is central to thermobaricity. The term $\partial\alpha^\Theta/\partial p$ is approximately constant with pressure for a given Θ; inversely related to Θ; positive for the oceanographically relevant ranges of Θ, S_A, and p; and an order of magnitude larger than $\partial\beta^\Theta/\partial p$. Through (1) and (5), it is clear that the pressure dependence of α^Θ will give rise to a pressure dependence of the density and spice stratifications, N^2 and K^2, respectively. From (1), this means that a water column that is stably stratified ($\alpha^\Theta\partial\Theta/\partial z > \beta^\Theta\partial S_A/\partial z$) at one pressure may be unstably stratified at another pressure ($\alpha^\Theta\partial\Theta/\partial z < \beta^\Theta\partial S_A/\partial z$; e.g., Fig. 3b). Additionally, from (5), a given heat and salt stratification ($\alpha^\Theta\partial\Theta/\partial z$, $\beta^\Theta\partial S_A/\partial z$) that results in an alpha ocean at one pressure could result in a beta ocean at a different pressure, and vice versa. Whether a given pressure perturbation is able to destabilize the stratification requires knowledge of both $\alpha^\Theta\partial\Theta/\partial z$ and $\beta^\Theta\partial S_A/\partial z$. For instance, an increase in pressure where ($\alpha^\Theta\partial\Theta/\partial z$, $\beta^\Theta\partial S_A/\partial z$) > 0 will increase N^2, while the same increase in pressure where ($\alpha^\Theta\partial\Theta/\partial z$, $\beta^\Theta\partial S_A/\partial z$) < 0 will decrease N^2. The pressure perturbation required to destabilize the stratification Δp can be estimated from the ratio of N^2 and its gradient with respect to pressure for fixed $\partial\Theta/\partial z$ and $\partial S_A/\partial z$, given as

$$\Delta p = \frac{\left(\alpha^\Theta\frac{\partial\Theta}{\partial z} - \beta^\Theta\frac{\partial S_A}{\partial z}\right)}{\left(\frac{\partial\alpha^\Theta}{\partial p}\frac{\partial\Theta}{\partial z} - \frac{\partial\beta^\Theta}{\partial p}\frac{\partial S_A}{\partial z}\right)}. \tag{16}$$

A similar equation can be derived to describe the pressure dependence of the spice stratification K^2 and can be used to estimate the pressure perturbation required to change ocean class. Recognizing that both N^2 and K^2 change with pressure and can act to destabilize or reclassify the water column, it is convenient to express the pressure influence on the stratification in Turner space as the gradient of Turner angle with pressure, $\partial\mathrm{Tu}/\partial p$. Given the thermal and saline dependence of α^Θ, this term depends on both Θ and S_A (and their respective vertical gradients), that is,

$$\left.\frac{\partial\mathrm{Tu}}{\partial p}\right|_{\Theta,S_A,\frac{\partial\Theta}{\partial z},\frac{\partial S_A}{\partial z}}. \tag{17}$$

Through this framework, if an oceanographically relevant change in pressure results in the Turner angle transitioning from $|\mathrm{Tu}| < \pi/2$ to $|\mathrm{Tu}| > \pi/2$, the water column itself is susceptible to thermobaric instability. This definition for thermobaric instability is referred to here as a type II instability.

The term in (17) can be calculated from the TEOS-10 functions analytically for a range of oceanographically relevant Θ and S_A values (here, $\Theta = 2.5°$, 25.0°C and $S_A = 34.0\,\mathrm{g\,kg^{-1}}$) and presented in Turner space (Figs. 4a,b). For $\pi/4 < |\mathrm{Tu}| < \pi/2$, increasing pressure decreases the Turner angle; that is, for gravitationally stable regions of $\mathrm{Tu} < -\pi/4$ (i.e., beta or transition zone oceans), an increase in pressure can result in $\mathrm{Tu} < -\pi/2$ and an unstable water column. Alternatively, a decrease in pressure in a gravitationally stable region with $\mathrm{Tu} > \pi/4$ (i.e., alpha or transition zone oceans) can lead to an unstable water column of $\mathrm{Tu} > \pi/2$. In the doubly stable region of $|\mathrm{Tu}| < \pi/4$, increasing (decreasing) pressure increases (decreases) the Turner angle toward $\mathrm{Tu} = \pi/4$ ($\mathrm{Tu} = -\pi/4$). In general, for an increase in pressure $\mathrm{Tu} = \pi/4$ is an attractor, while for a decrease in pressure $\mathrm{Tu} = -\pi/4$ is the attractor. Considering the inverse tangent relationship between (K^2, N^2) and Tu [(3), (6)], it is important to note that the trajectories of $\partial\mathrm{Tu}/\partial p$ in Turner space are hyperbolic and asymptote toward major axes; they do not simply rotate about the origin with constant radius. The Turner angles of cool waters are more sensitive to pressure variations than warmer waters; there is approximately an order of magnitude difference between the $\partial\mathrm{Tu}/\partial p$ fields calculated for

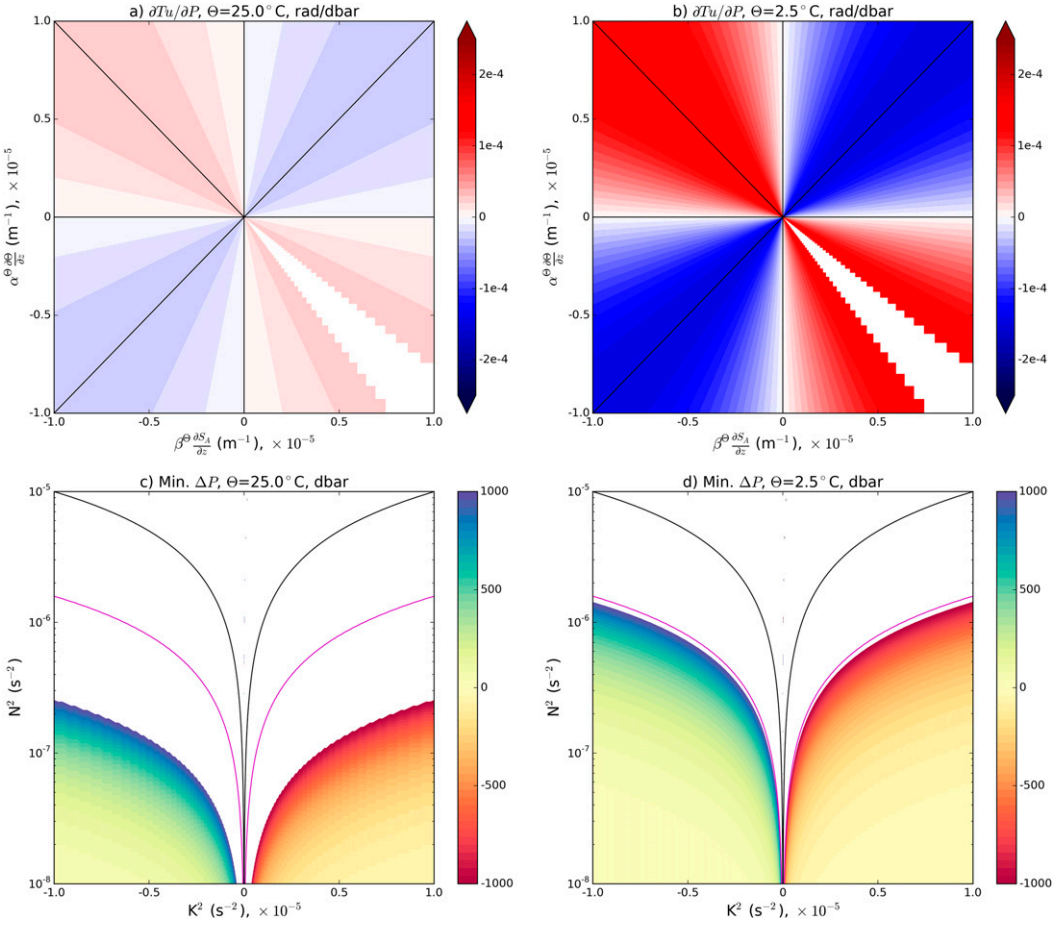

FIG. 4. The rate of change of Tu with pressure for (a) $\Theta = 25.0°C$ and (b) $\Theta = 2.5°C$ (for $S_A = 34\,g\,kg^{-1}$). The black contours indicate increasing values of Tu at $\pi/4$ increments from $Tu = -3\pi/4$ to $Tu = 3\pi/4$, clockwise from the bottom. The region in the vicinity of $Tu = \pm\pi$ is masked because of the change in sign. (c),(d) The minimum change in pressure required to destabilize a statically stable water column for a range of N^2 and K^2 with $\Theta = 25.0°C$ and $\Theta = 2.5°C$, respectively. The black contours indicate $Tu = \pm\pi/4$; the magenta contours show $Tu = \pm 9\pi/20$.

$\Theta = 2.5°C$ and $\Theta = 25.0°C$ (Figs. 4a,b). For the oceanographically relevant range, the influence of S_A variations on $\partial Tu/\partial p$ is negligible.

The gradient of stratification with respect to pressure provides an estimate of the minimum pressure change Δp required to destabilize a statically stable water column. It is useful to view this pressure change Δp in the (K^2, N^2) coordinate space shown in Fig. 2c. Variable Δp is negative for $Tu > \pi/4$, positive for $Tu < -\pi/4$, and undefined (because no value of Δp will generate thermobaric instabilities) for $|Tu| < \pi/4$ (Figs. 4c,d). The minimum pressure change Δp increases with increasing N^2 and decreasing K^2. For the oceanographically relevant example employed here, changes in pressure of more than ± 1000 dbar are needed for regions with $|Tu| \lesssim 9\pi/20$. Importantly, for a given N^2, the pressure change required to destabilize the water column is substantially less for cool waters relative to warm waters (Figs. 4c,d).

3. Hydrographic data

Static stability requires the potential density to increase with depth ($N^2 > 0$). This criterion is imposed for many hydrographic climatologies and reanalysis products, as well as hydrostatic numerical ocean models, which artificially modify the density field to meet it. While this static stability criterion does not necessarily eliminate thermobaric instabilities, it does reduce their prevalence and strength and hinders their detection. The Argo array of profiling floats provides near-global upper-ocean temperature and salinity data that remains unadjusted for static stability, making it ideal to identify thermobarically unstable water.

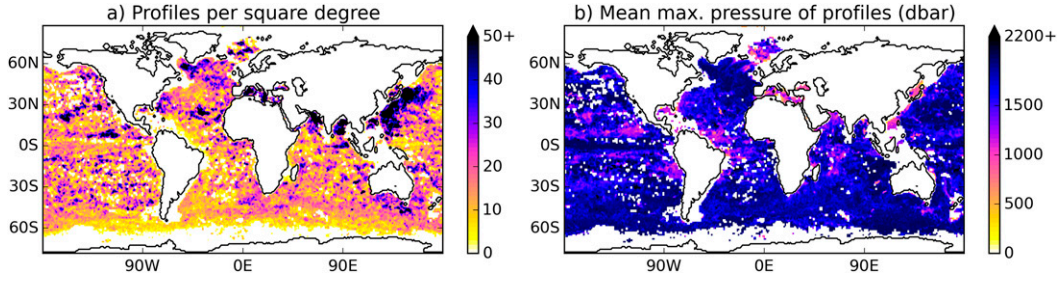

FIG. 5. Maps of (a) the global Argo float profile density (number of profiles per square degree, latitude × longitude) for 2010–13 and (b) the mean maximum pressure of these profiles.

Analyzed here are 4 years (2010–13) of hydrographic data that are developed primarily from the Argo array of profiling floats (Argo 2000). The data are obtained from the Ifremer website as both individual float profiles and global gridded products of upper-2-km ocean temperature and salinity. The individual float data average ~324 profiles per day for the period 2010–13, for a total of over 473 000 profiles. For the period 2010–13 the Argo float network averages a total of ~11 profiles per square degree (Fig. 5a), with an average maximum pressure of 1680 dbar (Fig. 5b) and steps in maximum pressure distribution at the equivalent of approximately 500-m intervals (presumably due to instrument programming). The distribution of Argo profiles is sparse poleward of the Bering Strait and Labrador and Norwegian Seas in the north and poleward of 60°S in the south (Fig. 5a). The global gridded product, primarily developed from the individual float data, uses the In Situ Analysis System (ISAS) methodology of Gaillard et al. (2009) to incorporate complementary data into regions undersampled by the Argo array; these complementary data are from a range of platforms including marine animals, moorings, drifting buoys, and thermosalinometers. These gridded fields are provided as monthly averages developed from the individual profiles and complementary data without imposing gravitational stability and at ~0.3° × 0.5° (latitude × longitude) horizontal resolution with vertical resolution of 3–20 m down to 2000 m (152 levels). Despite its relatively short duration, this particular hydrographic product was selected for its high vertical resolution, a useful feature for identifying thermobaric instabilities. Because of a reduction in the data coverage at depth,[4] the quantitative analysis of the gridded product is confined to the upper 1500 m, although the full profiles are qualitatively included in figures for completeness. The majority of the analysis presented here is derived from the gridded products; the individual float data were employed here as validation for these global fields.

The Turner angles and spice stratifications of the gridded products are calculated and used to define the alpha, beta, and transition zone oceans of the upper 2 km for 2010–13. Here, the complete 2010–13 period is used to calculate the average spice stratification and its standard deviation, $\overline{K^2}$ and σ_{K^2}, respectively [(5) and (9)]. The alpha, beta, and transition zone oceans are identified using (10)–(12). These classifications provide the basis for examining the upper-ocean type for distribution, stratification, and thermobaric stability.

4. Results and discussion

The gridded products are partitioned by ocean type [(10)–(12)]: the upper 1500 m is composed of approximately 67% alpha oceans, 15% beta oceans, and 17% transition zone oceans (Table 1). The distributions of the alpha, beta, and transition zone oceans have complicated horizontal and vertical structure (Figs. 6–8). For 2010–13, the upper ~50 m is almost entirely (>95%) transition zone oceans; this is presumably because the dominant contributor to the surface stratification is determined by the atmospheric, cryospheric, and radiative forcings, which all have strong seasonality [see the Tu analysis of mixed layer seasonality by Johnson et al. (2012)]. At a depth of 100 m, the fraction of alpha oceans is similar to that of transition zone oceans and the anticipated strong latitudinal distribution [alpha (beta) in low (high) latitudes] becomes apparent. The central regions of the major ocean gyres and Antarctic Circumpolar Current remain as transition zone oceans, however. At this depth, the beta oceans encompass the Arctic Ocean, Labrador Sea, and shelf waters near the Grand Banks, as well as the Okhotsk and Bering Seas, the Alaskan Gulf, and south of the sub-Antarctic Front (~60°S).

Beneath 400 m there is a strong contrast between the northern Pacific and Atlantic basins: beta oceans extend

[4] The value of σ_{K^2} becomes small or vanishes, indicating that only one or a few hydrographic measurements comprise the entire time series at that place.

TABLE 1. Definitions for alpha, beta, and transition zone oceans and the criteria used to identify type I thermobaric instabilities. Also shown by ocean type are the volume fractions (%) for the upper 1500 m of the global ocean and type I thermobarically unstable ocean and the average values of N^2 and K^2 for the upper 500 m.

	Alpha	Beta	Transition zone	Thermobaric instability
Definition	$\overline{K^2} - \sigma_{K^2} > 0$	$\overline{K^2} + \sigma_{K^2} < 0$	$\lvert\overline{K^2}\rvert - \sigma_{K^2} < 0$	(14), (15)
Percent of ocean	67.2	15.1	17.5	5.7
Percent of thermobarically unstable ocean	29.5	7.4	63.0	100
Average N^2 of upper 500 m (s^{-2})	1.02×10^{-4}	1.04×10^{-4}	2.91×10^{-5}	Global 6.06×10^{-5}
Average K^2 of upper 500 m (s^{-2})	1.06×10^{-4}	-9.93×10^{-5}	9.92×10^{-6}	Global 5.08×10^{-5}

poleward of 45°N in the Pacific, and yet no longer exist in the Atlantic (Figs. 6–8). The southern beta ocean extends equatorward from the Antarctic continental shelf (evident in the meridional transects, Fig. 7). The alpha oceans account for approximately 80% of the global oceans by 400 m, and the southern extent of the low-latitude alpha oceans links the major basins. For the Pacific and Indian (Atlantic) Oceans this border approximately aligns with the $\sigma_0 = 27.4\,\mathrm{kg\,m^{-3}}$ ($27.2\,\mathrm{kg\,m^{-3}}$) isopycnal. It is farthest north immediately east (downstream) of Drake Passage (~40°S), gradually shifting poleward to the east so as to pass south of Africa and New Zealand, eventually intersecting Cape Horn. This circumpolar continuity is mirrored in the southern beta oceans; zonal transects indicate the beta ocean is shallowest east of Drake Passage and gradually deepens to the east (Fig. 8). This eastward deepening of the southern beta oceans is also apparent in the depths of the beta ocean equatorward intrusions into the major basins; these are at ~1 km in the Atlantic and ~1.5 km in the Indian and Pacific (Fig. 7). The structure of the ocean type boundaries resembles the sloping of

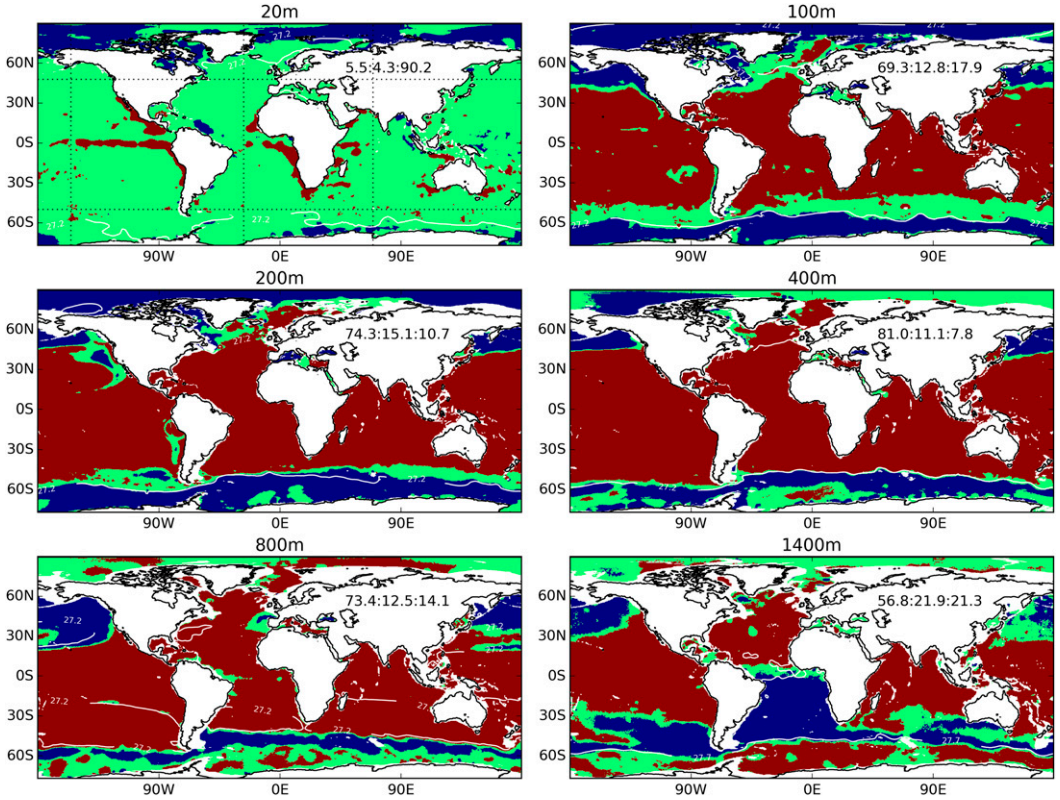

FIG. 6. The global distributions of alpha (red), beta (blue), and transitions zone (green) oceans calculated from the gridded product for 2010–13 for six depths. The numbers across Eurasia indicate the alpha, beta, and transition zone ocean percentages at each depth. The dotted lines on the 20-m panel indicate the locations of the vertical transects in Figs. 7 and 8. Contours of the 2010–13 average σ_0 isopycnals are shown in white. Regions where $\sigma_{K^2} = 0$ are masked.

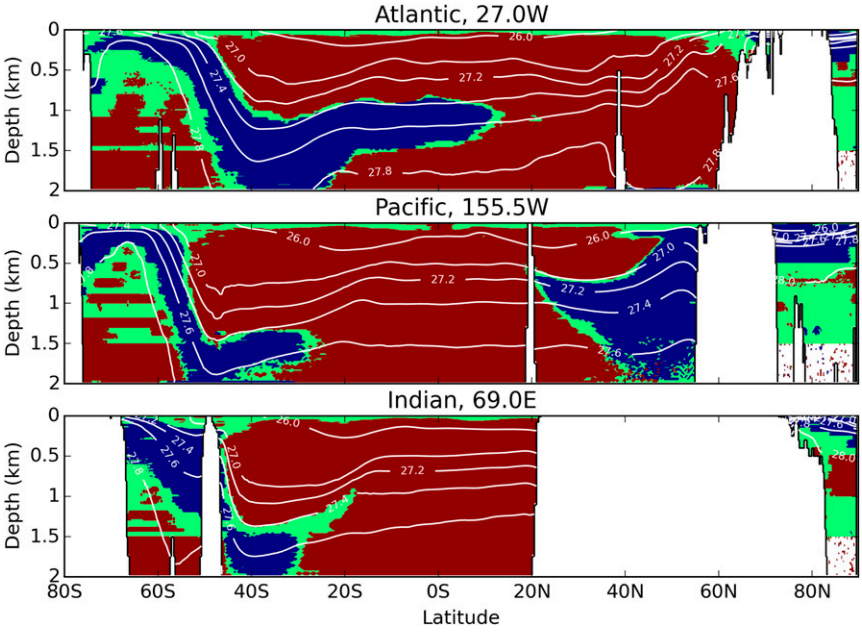

FIG. 7. Meridional transects of the alpha (red), beta (blue), and transitions zone (green) ocean distributions calculated from the gridded product for 2010–13. Contours of the 2010–13 average σ_0 isopycnals are shown in white. Regions where $\sigma_{K^2} = 0$ are masked.

isopycnal surfaces (Figs. 7, 8). A similar beta ocean equatorward intrusion exists in the northern Pacific, although at a much shallower depth (~500 m); it is absent in the northern Atlantic Ocean. The transition zone oceans surrounding these beta ocean intrusions coincide with the fresh-tongue signatures of Antarctic Intermediate Water and North Pacific Intermediate Water. For depths greater than ~1 km, a subsurface alpha ocean exists along the Antarctic continental slope; it is possibly connected to the equatorial alpha ocean at depths greater than 2 km, but this cannot be confirmed with Argo data.

Globally, 2.28% of the gridded product seawater volume is gravitationally unstable. This is most apparent in the $N^2 < 0$ regions of the Turner space volumetric distributions for the upper 1500 m (Fig. 9). Here, the global preference for alpha oceans is also evident (upper panels of Fig. 9). Distinguishing between the ocean types highlights the distinct differences in the prevalence of gravitational instabilities for alpha, beta, and transition zone oceans. Specifically, 0.83% of alpha oceans, 0.98% of beta oceans, and 8.9% of transition zone oceans are gravitationally unstable (lower panels of Fig. 9).

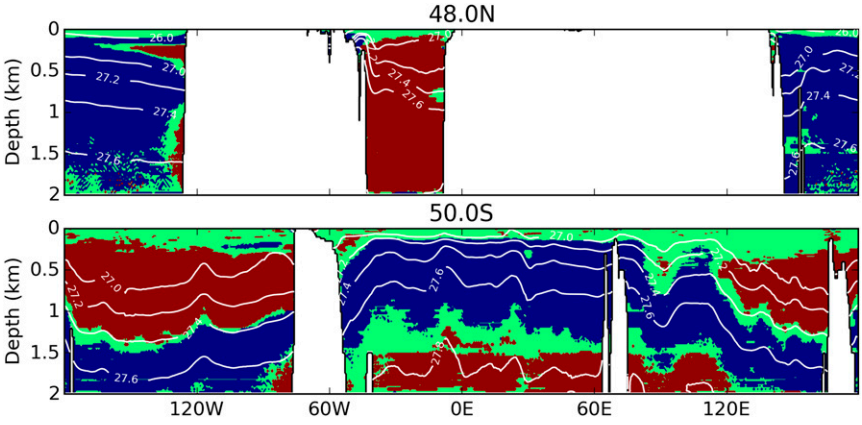

FIG. 8. As in Fig. 7, but for zonal transects.

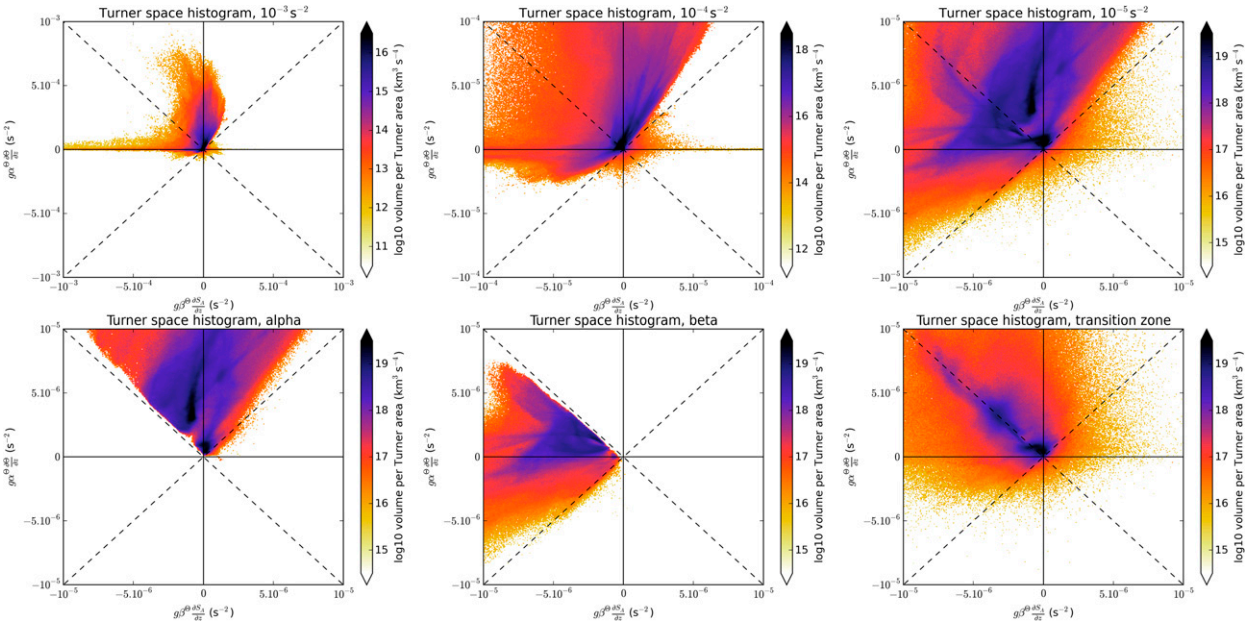

FIG. 9. The Turner space volumetric distribution of the 2010–13 mean of the gridded product: (top) progressively zooms in on the origin to the right and (bottom) the Turner space distributions for the alpha, beta, and transition zone oceans, at the scale of the upper right figure (see axis scales). Note the change in the color scales between panels.

Viewing the ocean volumetric distribution in Turner space offers an insightful perspective to the global density stratification (Fig. 9). The dominance of the heat stratification is evident for the strongly through to weakly stratified regions (upper panels, Fig. 9), as well as transition zone oceans (lower right, Fig. 9). Boundaries of preferred Turner angles are evident; interestingly, one such boundary appears to lie along Tu = $9\pi/20$, the oceanographically relevant limit for type II thermobaric instabilities (Figs. 4c,d). The volumetric distributions of alpha and beta oceans in Turner space hint at the existence of overturning circulations within these ocean classes, that is, circulations within alpha and beta oceans driven by heat and salt/freshwater, respectively, where the secondary property (salt and heat, respectively) is dynamically passive. A thorough examination of such overturning circulations will require a full depth ocean dataset and will be the focus of future work.

The prevalence of gravitational instability in transition zone oceans is also evident in a more conventional representation of ocean stratification when viewed by ocean type and stratifying species (Fig. 10). This analysis identifies the regions where the oceans are unstably stratified by either temperature (Fig. 10a) or salinity (Fig. 10b). Notably, the global ocean is, on average, unstably stratified by salt between ~150 and 800 m. Alpha oceans are also unstably stratified by salt at the surface and between ~100 and 1000 m, and beta oceans tend to be unstably stratified by temperature between ~100 and 400 m. Transition zone oceans are on average stable in both heat and salt at all depths, although they are the weakest stratified regions of the ocean types, with an average $N^2 = 2.91 \times 10^{-5}\,\mathrm{s}^{-2}$ for the upper 500 m compared to 1.02×10^{-4} and $1.04 \times 10^{-4}\,\mathrm{s}^{-2}$ for alpha and beta oceans, respectively, and the global average of $6.06 \times 10^{-5}\,\mathrm{s}^{-2}$ (Fig. 10c, Table 1). This weak stratification makes transition zone oceans ideal locations for efficiently coupling surface waters to the deep, a trait that is also reflected by their tendency to be gravitationally unstable. Interestingly, this analysis suggests the strongest stratification occurs at the surface of beta oceans.

The spice stratification K^2 is of similar absolute magnitude as N^2 (Fig. 10d, Table 1). As in the case of N^2, the transition zone oceans have the weakest spice stratification with an average of $K^2 = 9.92 \times 10^{-6}\,\mathrm{s}^{-2}$ for the upper 500 m; the values for alpha and beta oceans are 1.06×10^{-4} and $-9.93 \times 10^{-5}\,\mathrm{s}^{-2}$, respectively, and the global average is $5.08 \times 10^{-5}\,\mathrm{s}^{-2}$. For depths below ~200 m, the absolute value of the transition zone ocean spice stratification is approximately an order of magnitude smaller than that of alpha, beta, and the global ocean average (Fig. 10d). Both the global average and transition zone ocean spice stratifications tend to be positive, indicating they are closer to alpha oceans than beta oceans.

By the type I instability criterion of (15), 5.7% of the gravitationally stable global oceans are thermobarically unstable for water parcel relocations; this is composed

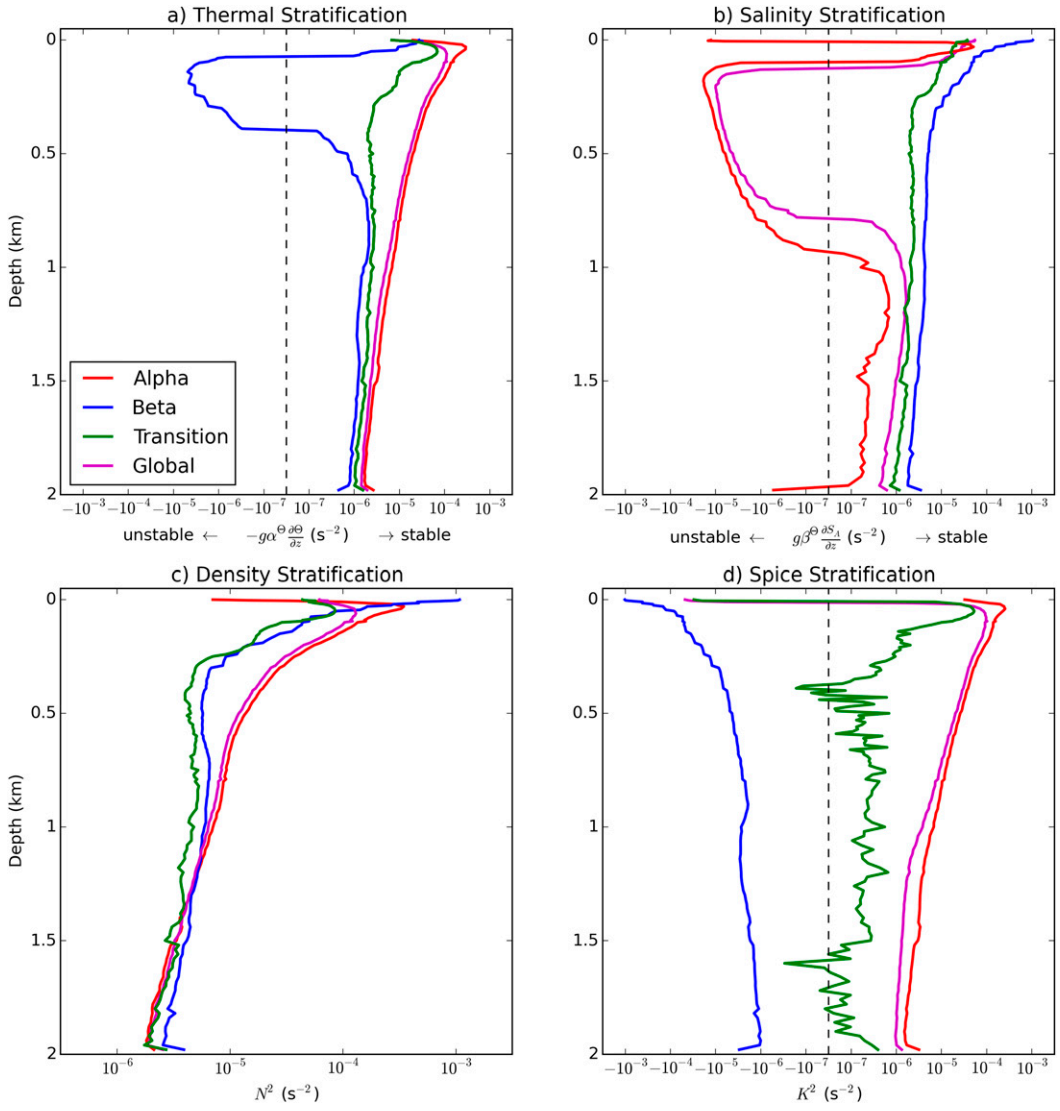

FIG. 10. The average (a) thermal, (b) salinity, (c) density, and (d) spice stratifications for the global (magenta), alpha (red), beta (blue), and transition zone (green) oceans with depth. The dashed lines indicate where the abscissa logarithmic scale passes through zero.

of 2.5% of the alpha oceans, 2.8% of the beta oceans, and 20.6% of the transition zone oceans. The standout result here is that despite containing only 17% of the global upper-ocean volume, the transition zone oceans account for over 63% of the thermobaric instabilities (Table 1). This tendency for the transition zone oceans to be thermobarically unstable is most apparent when comparing the vertical distributions of ocean composition for the global and thermobarically unstable oceans (Fig. 11). As evident in the spatial distributions of ocean compositions (Figs. 6–8), the dominant ocean type shifts from transition zone to alpha oceans around 100 m depth (Fig. 11a). Given this dominance of transition zone oceans in the upper 100 m, and its tendency to be thermobarically unstable, it makes sense that a large fraction (almost 60%) of surface waters are thermobarically unstable (Fig. 11b). This fraction of unstable ocean waters decreases to ~5% by 200 m depth; for transition zone oceans this large fraction remains around 20% down to 800 m and ~15% below this. Restricting the ocean composition analysis to the thermobarically unstable waters only reveals that virtually all unstable surface waters are in transition zone oceans (Fig. 11c), with this fraction decreasing to about 40% down to 200 m, where it steadily increases back to the upper-ocean average of ~60%.

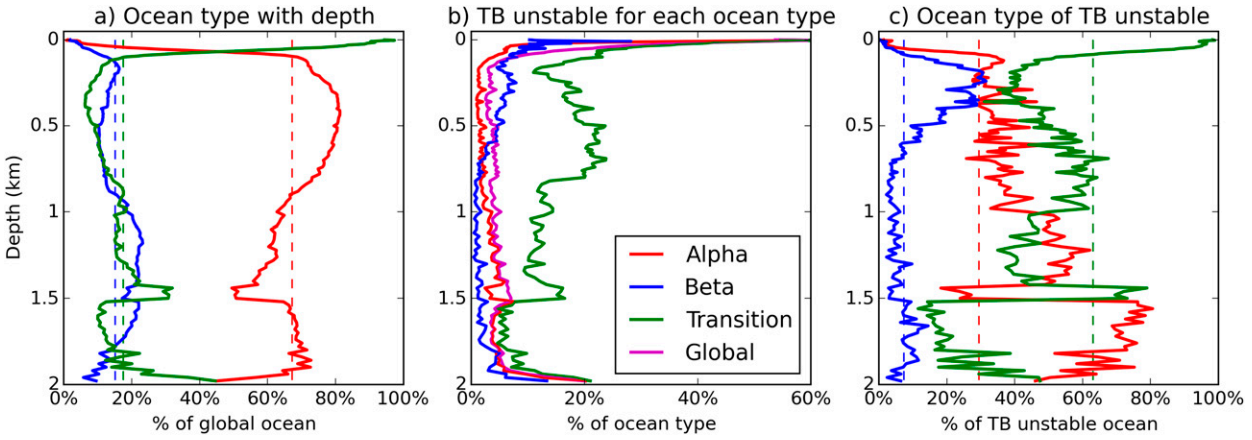

FIG. 11. (a) Vertical profiles of the percentage of the global ocean volume that are alpha (red), beta (blue), and transition zone (green) oceans with depth. The discontinuities at 0.5, 1.0, 1.5, and 2.0 km correspond with peaks in the distribution of maximum depths of individual float profiles. The dashed lines are the global averages of the upper 1500 m. (b) Vertical profiles of the percentage of each ocean type that is thermobarically unstable. (c) Vertical profiles of the percentage of thermobarically unstable water that are alpha, beta, and transition zone oceans with depth. The dashed lines are the global averages of the upper 1500 m. While the transition zone oceans contain only 17% of the total volume (a), they account for over 63% of the thermobarically unstable waters (c). Note that (b) and (c) are conditional statistics: the percentages in (b) are calculated for each ocean type and in (c) for thermobarically unstable waters only.

Despite their vast volumetric differences (Fig. 11a), the alpha and beta oceans have comparable contributions to thermobaric instabilities down to ~400 m, below which the beta ocean contributions reduce to around 10%. Thermobaric instabilities continue to be predominantly located in transition zone oceans down to 1 km, where the alpha ocean contribution increases to become comparable. Figure 11 highlights the sudden reduction in data quality below 1500 m.

The spatial distribution of thermobaric instabilities exhibits seasonal variability in the upper 400 m, tending to be more active during the local winter (Figs. 12a–d). As noted in the vertical distributions (Figs. 11b,c), the upper ocean is more susceptible to type I thermobaric instability arising from water parcel relocation (cf. Figs. 12a,b with Figs. 12c,d); this makes good physical sense given the surface dominance of transition zone oceans.

Type II thermobaric instabilities can be diagnosed by examining the pressure dependence of the stratification [(16), (17)]. This diagnostic provides an estimate of the minimum change in pressure needed to destabilize the stratification and suggests that stratification of the majority of the surface oceans ($z < 60$ m) will remain stable for oceanographically realistic pressure perturbations. Exceptions to this are during the local winters in Baffin Bay; the Labrador, Bering, and Okhotsk Seas; and multiple locations on and surrounding the Antarctic shelf (Figs. 12e,f). By 200 m depth, the seasonal variability of this diagnostic has reduced and the thermobarically susceptible regions are primarily in the high latitudes poleward of 50°S, and in particular the Weddell Sea, the Bering and Labrador Seas, and the central Arctic Ocean (Figs. 12g,h). This suggests that these cool, beta ocean regions require pressure increases of $O(100)$ dbar for their stratifications to become unstable. Considering the $O(1000)$ m mixed layer depths in some of these regions, this diagnostic is useful for identifying type II thermobaric instabilities in these high-latitude waters. In other regions, however, the change in pressure required to destabilize the stratification is beyond that of oceanographic relevance (i.e., extending beyond the available range of the water column).

Interestingly, type I and II thermobaric instabilities are not necessarily collocated. While type I instabilities are surface intensified (Fig. 11b), the vertical distribution of type II exhibits an intermediate depth maximum of ~6.4% around 200 m deep (Table 2). Overall, for the purpose of this and other global ocean studies, the identification of type I instabilities is more applicable than type II; however, the latter should not be discounted, especially in high-latitude oceans.

5. Conclusions

The locally dominant stratifying property of seawater (heat or salt) is an important, underappreciated ocean characteristic that is of fundamental climatic influence. Here, it is used to classify the oceans into alpha, beta, and transition zone oceans, which are subsequently examined for thermobaric instabilities. Analysis of hydrographic data primarily developed from Argo

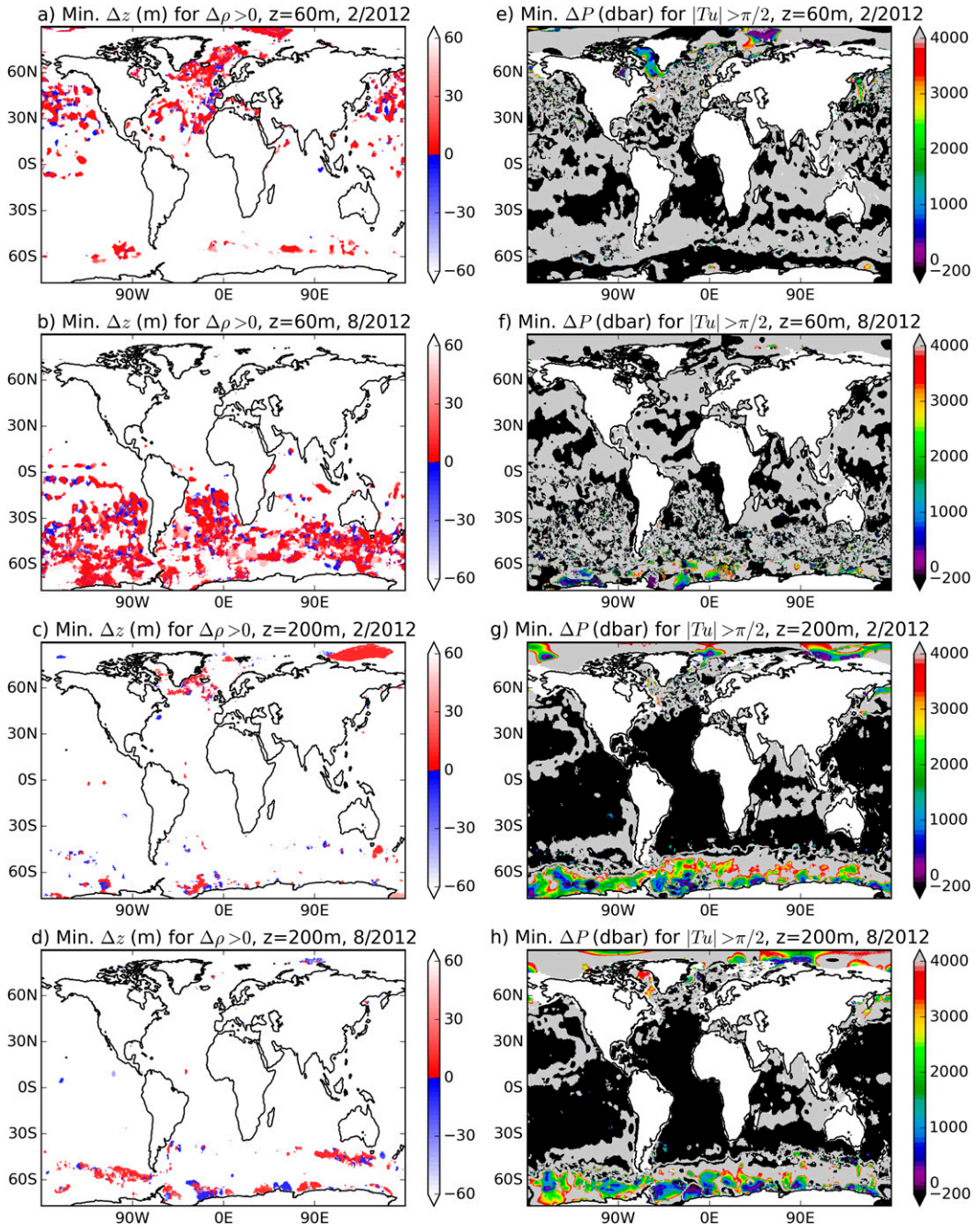

FIG. 12. (left) The minimum change in depth required for water parcels at (a),(b) $z = 60$ m and (c),(d) $z = 200$ m to become thermobarically unstable during (a),(c) February and (b),(d) August of 2012. Here, red is sinking and blue is shoaling, and the white regions are thermobarically stable to type I instabilities. (right) The minimum pressure change required for type II instabilities to destabilize the stratification at (e),(f) $z = 60$ m and (g),(h) $z = 200$ m during (e),(g) February and (f),(h) August of 2012. The offscale black regions indicate where the (upward) pressure change is greater than that at z, and the gray regions indicate where the (downward) pressure change is greater than that equivalent to 4000 m. The percentages of the thermobarically unstable waters here are listed in Table 2.

TABLE 2. Percentage of type I and II thermobarically unstable water at $z = 60$, 200 m for February and August 2012, depicted in Fig. 12.

	February		August	
Depth	60 m	200 m	60 m	200 m
Type I	11.1	2.9	24.5	4.2
Type II	2.2	6.5	3.6	6.3

profiling floats reveals the composition, and distribution of alpha, beta, and transition zone oceans have complicated horizontal and vertical structure. The surface waters are predominantly transition zone oceans, likely because of the seasonal variability in surface forcing. By 100 m depth alpha oceans dominate. Despite occupying only 17% of the upper 1500 m ocean volume, transition zone oceans contain over 63% of the thermobarically unstable waters. They are the most weakly stratified regions of the global oceans and contain 69% of the gravitationally unstable water. Thermobarically unstable water is 2.6 times more abundant than gravitationally unstable water. These facts make the transition zone oceans ideal locations for efficiently coupling the surface waters with the deep through enhanced vertical transport of water-mass properties. Future work with high-resolution ocean models will illuminate the role of transition zone oceans in the vertical fluxes of heat and water masses, as well as the potential energy associated with thermobaric instabilities. In addition, future work should quantify secular change in thermobaricity and the distribution of alpha and beta oceans. It should also address the physical processes controlling their properties.

Acknowledgments. The individual float and gridded ISAS data (Gaillard et al. 2009) were obtained from the Ifremer website (ftp://ftp1.ifremer.fr/Core/, downloaded 29 July 2015). Many thanks to A. Hogg, R. Griffiths, J. Saenz, C. Shakespeare, and J. Nycander for very helpful discussions. The authors greatly appreciate the helpful reviews from an anonymous reviewer and J. Zika, who suggested a statistical definition for the ocean type classifications.

REFERENCES

Argo, 2000: Argo float data and metadata from Global Data Assembly Centre (Argo GDAC). Ifremer, accessed 2 May 2016, doi:10.12770/1282383d-9b35-4eaa-a9d6-4b0c24c0cfc9.

Akitomo, K., 1999a: Open-ocean deep convection due to thermobaricity: 1. Scaling argument. *J. Geophys. Res.*, **104**, 5225–5234, doi:10.1029/1998JC900058.

——, 1999b: Open-ocean deep convection due to thermobaricity: 2. Numerical experiments. *J. Geophys. Res.*, **104**, 5235–5249, doi:10.1029/1998JC900062.

Carmack, E., 2007: The alpha/beta ocean distinction: A perspective on freshwater fluxes, convection, nutrients and productivity in high-latitude seas. *Deep-Sea Res. II*, **54**, 2578–2598, doi:10.1016/j.dsr2.2007.08.018.

——, W. Williams, S. Zimmermann, and F. McLaughlin, 2012: The Arctic Ocean warms from below. *Geophys. Res. Lett.*, **39**, L07604, doi:10.1029/2012GL050890.

Fedorov, A., R. Pacanowski, S. Philander, and G. Boccaletti, 2004: The effect of salinity on the wind-driven circulation and the thermal structure of the upper ocean. *J. Phys. Oceanogr.*, **34**, 1949–1966, doi:10.1175/1520-0485(2004)034<1949:TEOSOT>2.0.CO;2.

Fofonoff, N., 1961: Energy transformations in the sea. Fisheries Research Board of Canada Manuscript Report Series, Vol. 109, 82 pp.

Franco, A., and Coauthors, 2014: Air-sea CO_2 fluxes above the stratified oxygen minimum zone in the coastal region off Mexico. *J. Geophys. Res. Oceans*, **119**, 2923–2937, doi:10.1002/2013JC009337.

Gaillard, F., E. Autret, V. Thierry, P. Galaup, C. Coatanoan, and T. Loubrieu, 2009: Quality control of large Argo data sets. *J. Atmos. Oceanic Technol.*, **26**, 337–351, doi:10.1175/2008JTECHO552.1.

Garwood, R., S. Isakari, and P. Gallacher, 1994: Thermobaric convection. *The Polar Oceans and Their Role in Shaping the Global Environment*, *Geophys. Monogr.*, Vol. 85, Amer. Geophys. Union, 199–209.

Haine, T., and J. Marshall, 1998: Gravitational, symmetric, and baroclinic instability of the ocean mixed layer. *J. Phys. Oceanogr.*, **28**, 634–658, doi:10.1175/1520-0485(1998)028<0634:GSABIO>2.0.CO;2.

Hieronymus, M., and J. Nycander, 2015: Finding the minimum potential energy state by adiabatic parcel rearrangements with a nonlinear equation of state: An exact solution in polynomial time. *J. Phys. Oceanogr.*, **45**, 1843–1857, doi:10.1175/JPO-D-14-0174.1.

Hughes, G., A. Hogg, and R. Griffiths, 2009: Available potential energy and irreversible mixing in the meridional overturning circulation. *J. Phys. Oceanogr.*, **39**, 3130–3146, doi:10.1175/2009JPO4162.1.

IOC, SCOR, and IAPSO, 2010: The international thermodynamic equation of seawater–2010: Calculation and use of thermodynamic properties. Manuals and Guides, Vol. 56, Intergovernmental Oceanographic Commission, UNESCO, 196 pp. [Available online at http://unesdoc.unesco.org/images/0018/001881/188170e.pdf.]

Johnson, G., S. Schmidtko, and J. Lyman, 2012: Relative contributions of temperature and salinity to seasonal mixed layer density changes and horizontal density gradients. *J. Geophys. Res.*, **117**, C04015, doi:10.1029/2011JC007651.

Klocker, A., and T. McDougall, 2010: Influence of the nonlinear equation of state on global estimates of dianeutral advection and diffusion. *J. Phys. Oceanogr.*, **40**, 1690–1709, doi:10.1175/2010JPO4303.1.

McDougall, T., 1987: Thermobaricity, cabbeling, and water-mass conversion. *J. Geophys. Res.*, **92**, 5448–5464, doi:10.1029/JC092iC05p05448.

McLaughlin, F., and E. Carmack, 2010: Deepening of the nutricline and chlorophyll maximum in the Canada Basin interior, 2003–2009. *Geophys. Res. Lett.*, **37**, L24602, doi:10.1029/2010GL045459.

McPhee, M., 2000: Marginal thermobaric stability in the ice-covered upper ocean over Maud Rise. *J. Phys. Oceanogr.*, **30**, 2710–2722, doi:10.1175/1520-0485(2000)030<2710:MTSITI>2.0.CO;2.

——, 2003: Is thermobaricity a major factor in Southern Ocean ventilation? *Antarct. Sci.*, **15**, 153–160, doi:10.1017/S0954102003001159.

Munk, W., 1981: Internal waves and small-scale processes. *Evolution of Physical Oceanography—Scientific Surveys in Honor of Henry Stommel*, B. Warren and C. Wunsch, Eds., MIT Press, 264–291.

Nycander, J., M. Hieronymus, and F. Roquet, 2015: The nonlinear equation of state of sea water and the global water mass distribution. *Geophys. Res. Lett.*, **42**, 7714–7721, doi:10.1002/2015GL065525.

Polyakov, I., A. Pnyushkov, R. Rember, L. Padman, E. Carmack, and J. Jackson, 2013: Winter convection transports Atlantic water heat to the surface layer in the eastern Arctic ocean. *J. Phys. Oceanogr.*, **43**, 2142–2155, doi:10.1175/JPO-D-12-0169.1.

Roden, G., 1970: Aspects of the mid-Pacific transition zone. *J. Geophys. Res.*, **75**, 1097–1109, doi:10.1029/JC075i006p01097.

Rooth, C., 1982: Hydrology and ocean circulation. *Prog. Oceanogr.*, **11**, 131–149, doi:10.1016/0079-6611(82)90006-4.

Ruddick, B., 1983: A practical indicator of the stability of the water column to double-diffusive activity. *Deep-Sea Res. I*, **30**, 1105–1107, doi:10.1016/0198-0149(83)90063-8.

Saenz, J., R. Tailleux, E. Butler, G. Hughes, and K. Oliver, 2015: Estimating Lorenz's reference state in an ocean with a nonlinear equation of state for seawater. *J. Phys. Oceanogr.*, **45**, 1242–1257, doi:10.1175/JPO-D-14-0105.1.

Stewart, K., J. Saenz, A. Hogg, G. Hughes, and R. Griffiths, 2014: Effect of topographical barriers on the rates of available potential energy conversion of the oceans. *Ocean Modell.*, **76**, 31–42, doi:10.1016/j.ocemod.2014.02.001.

Sverdrup, H., M. Johnson, and R. Fleming, 1942: *The Oceans: Their Physics, Chemistry, and General Biology*. Prentice-Hall, 1087 pp.

Talley, L., and J. Yun, 2001: The role of cabbeling and double diffusion in setting the density of the north Pacific intermediate water salinity minimum. *J. Phys. Oceanogr.*, **31**, 1538–1549, doi:10.1175/1520-0485(2001)031<1538:TROCAD>2.0.CO;2.

Urakawa, L., J. Saenz, and A. Hogg, 2013: Available potential energy gain from mixing due to the nonlinearity of the equation of state in a global ocean model. *Geophys. Res. Lett.*, **40**, 2224–2228, doi:10.1002/grl.50508.

You, Y., 2002: A global ocean climatological atlas of the Turner angle: Implications for double-diffusion and water mass structure. *Deep-Sea Res. I*, **49**, 2075–2093, doi:10.1016/S0967-0637(02)00099-7.

——, N. Suginohara, M. Fukasawa, I. Yasuda, I. Kaneko, H. Yoritaka, and M. Kawamiya, 2000: Roles of the Okhotsk Sea and Gulf of Alaska in forming the North Pacific intermediate water. *J. Geophys. Res.*, **105**, 3253–3280, doi:10.1029/1999JC900304.